An approximation to the PTT viscoelastic model for Gas Assisted Injection Moulding simulation

P. Olley*

Department of Mechanical and Energy Systems Engineering, Faculty of Engineering & Informatics, University of Bradford, Bradford, BD7 1DP, UK

email: P.Olley@bradford.ac.uk

Abstract: An approximation to the Phan-Thien Tanner (PTT) constitutive model is developed with the aim of giving low-cost simulation of Gas Assisted Injection Moulding (GAIM) while incorporating important viscoelastic characteristics. It is shown that the developed model gives a response typical of full viscoelastic models in transient and steady-state uniaxial and constant shear rate deformations. The model is incorporated into a 3D finite element GAIM simulation which uses the 'pseudo-concentration' method to predict residual polymer, and applied to published experimental results for a Boger fluid and a shear-thinning polystyrene melt.

It is shown that the simulation gives a very good match to published results for the Boger fluid which show increasing Residual Wall Thickness (RWT) with increasing Deborah number. Against the shear-thinning polymer, the quality of match depends upon which of two 'plausible' relaxation times is chosen; qualitatively different results arise from two different means of estimating a single relaxation time. A 'multi-mode' approach is developed to avoid this uncertainty. It is shown that the multi-mode approach gives decreasing RWT with increasing Deborah number in agreement with the published experimental results, and avoids the issues that arise from estimating a single relaxation time for a molten polymer.

Keywords: Gas Assisted Injection Moulding, PTT approximation, Residual Wall Thickness

1. Introduction and background

The Gas Assisted Injection Moulding (GAIM) process is a method for producing hollowed out plastic components that uses an initial part-injection of molten polymer followed by an injection of high pressure gas to complete the packing and to leave a hollow core [1, 2]. The advantages over conventional injection moulding can be considerable: lightweight parts with reduced material usage, quicker cooling and so higher production rates, reduced shrinkage marks as the gas pressure can be maintained during cooling and the consequent shrinking, and reduced residual stresses. Structural rigidity and tensile strength is also good compared with conventional injection moulding [3, 4]. The primary disadvantages are that more complex production tools are required and it is more difficult to predict final dimensions due to the complex behaviour of the gas-polymer interface that results. In particular the prediction of Residual Wall Thickness (RWT) is complex and has been the target of much study.

GAIM has been studied using both Lagrangian type moving mesh approaches and Eulerian type pseudo-concentration methods. Both of these approaches allow the incorporation of much relevant physics into the simulation. Techniques that are closely related to GAIM are

Water Assisted Injection Moulding (WAIM) [5], and Fluid Assisted Injection Moulding (FAIM) [6] which can use gas, water or oil as the secondary injection fluid. Comparable two phase viscoelastic or viscoplastic studies have been made for: removal of a viscoplastic fluid from pipes using a Newtonian phase [7, 8], cement casing [9], fibre orientation [10], and centrifugal spinning with nanofibres [11]. Constitutive models for the non-Newtonian component in GAIM and comparable flows have included the Power Law [1, 2], Cross-WLF [12, 13], Modified Maxwell Model [14], Doi-Edwards (D-E) [15], KBKZ [16, 17], Phan-Thien Tanner (PTT) [15, 18], generalised multi-mode differential model [19], Molecular Stress Function (MSF) [15, 20] and eXtended Pom-Pom (XPP) models [21]. Of these the Power Law model brings instantaneous shear-thinning behaviour to simulations and the Cross-WLF brings additional temperature dependence. The remaining viscoelastic models bring elasticity into simulations, which has been shown to be important in determining the propagation of the polymer-gas interface in GAIM simulations [15, 18].

It is clear from the research that viscoelastic models capture important transient elasticity in a polymer-gas flow and are preferred for more realistic simulation, but it is also widely appreciated that simulation using viscoelastic models can be exceptionally computationally expensive. This expense can be prohibitive for “real world” engineering problems as they tend to be geometrically complex and so usually require a complex 3D simulation; this is in addition to needing a large number of small time steps to track the progress of the phases accurately. This problem motivates the current work to produce an approximation to the popular PTT model that has a low computational cost, and assess it against some well characterised problems that involve predicting the Residual Wall Thickness (RWT) of a GAIM type flow.

2. Phan-Thien Tanner Approximation Model

The Phan-Thien Tanner (PTT) model can be written

$$\lambda\left(\frac{D\boldsymbol{\tau}}{Dt}-\boldsymbol{\tau}.\nabla\mathbf{u}-\nabla\mathbf{u}^{\mathrm{T}}.\boldsymbol{\tau}\right)+\boldsymbol{\tau}\exp\left(\frac{\varepsilon\lambda\,trace(\boldsymbol{\tau})}{\eta_0}\right)=\eta_0\,\dot{\boldsymbol{\gamma}} \qquad (1)$$

where $\boldsymbol{\tau}$ is the viscoelastic stress tensor, $\dot{\boldsymbol{\gamma}}$ is the rate of strain tensor, η_0 is the low-rate viscosity of the polymer , $\mathbf{u}$ is the velocity vector, λ is a characteristic time of the polymer and ε is a parameter which controls the rate dependence of the viscoelastic stress. In 3-D this model naturally expands out to give nine evolution equations for the nine stress components; symmetry of the stress tensor reduces this count to six independent equations for computational purposes. In order to reduce computation costs while maintaining significant viscoelastic effects, consider the following scalar approximation of the full PTT model:

$$\lambda\frac{D\bar{\tau}}{Dt}+\bar{\tau}\exp\left(\frac{\varepsilon\lambda\bar{\tau}}{\eta_0}\right)=\eta_0\bar{\dot{\gamma}} \qquad (2)$$

where $\bar{\tau}$ is a scalar measure of the viscoelastic stress, and $\bar{\dot{\gamma}}$ is a scalar measure of the deformation rate given by

$$\bar{\dot{\gamma}} = \sqrt{\frac{1}{2}\dot{\boldsymbol{\gamma}} : \dot{\boldsymbol{\gamma}}^{\mathrm{T}}} \tag{3}$$

If the stress measure $\bar{\tau}$ is calculated within a flow by time-stepping Eq. 2 then a local value of apparent polymer viscosity, μ_a can be obtained from

$$\mu_a = \bar{\tau} \big/ \bar{\dot{\gamma}}, \tag{4}$$

and these local values of apparent viscosity can be used for the next time-step of a time-stepping Navier-Stokes type simulation.

The transient viscosities for shear and uniaxial deformations that arise from this method are shown in Fig. 1 for a range of rates. The results are for a characteristic time constant of 1 sec, low rate viscosity (η_0) of 1 Pas and an ε value of 0.01. The approximation retains several important aspects of the full PTT model: a gradual rise of apparent viscosity with time to a plateau value; and rate dependence which can be controlled by the parameter ε. In addition the plateau value at low-rates is equal to the low-rate viscosity in shear, and a factor of 3 higher in uniaxial deformation, as expected from the full PTT model.

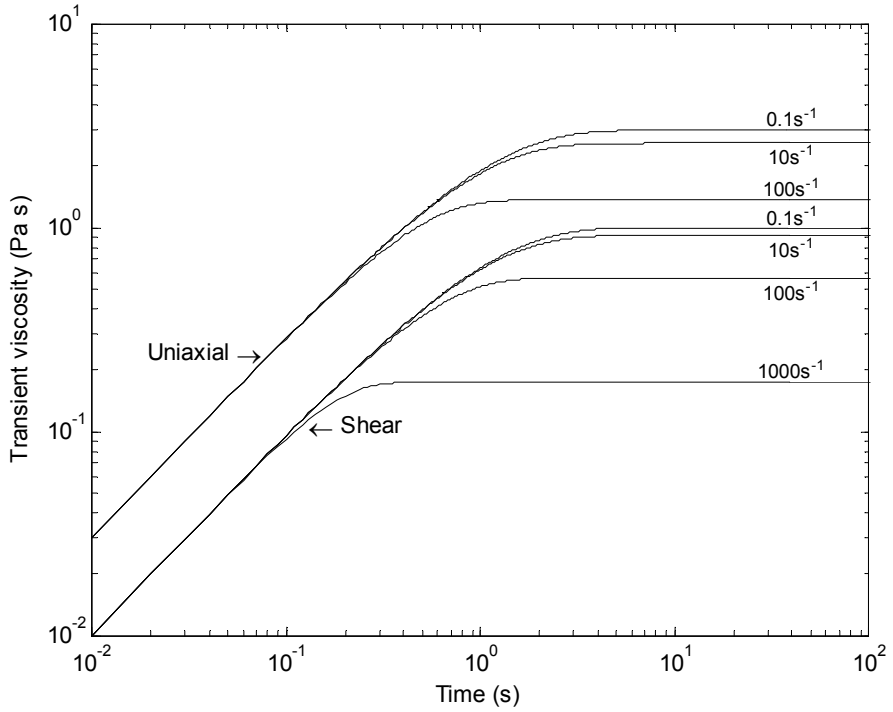

Figure 1 Transient viscosity in shear and uniaxial deformation given by Eq. (2)

In direct comparison with the full PTT model the approximation shows a number of simplifications in behaviour. Figure 2 shows a comparison of uniaxial and shear response of

the two models with a time constant of 2.2 seconds and an ε value of 1.3 for the PTT approximation (equal to values used later in this work for an actual polymer). A value of ε = 1.3 was also used for the full PTT model as it gives a comparable range. A low-rate shear viscosity (η_0) of 1Pa s was used for both models.

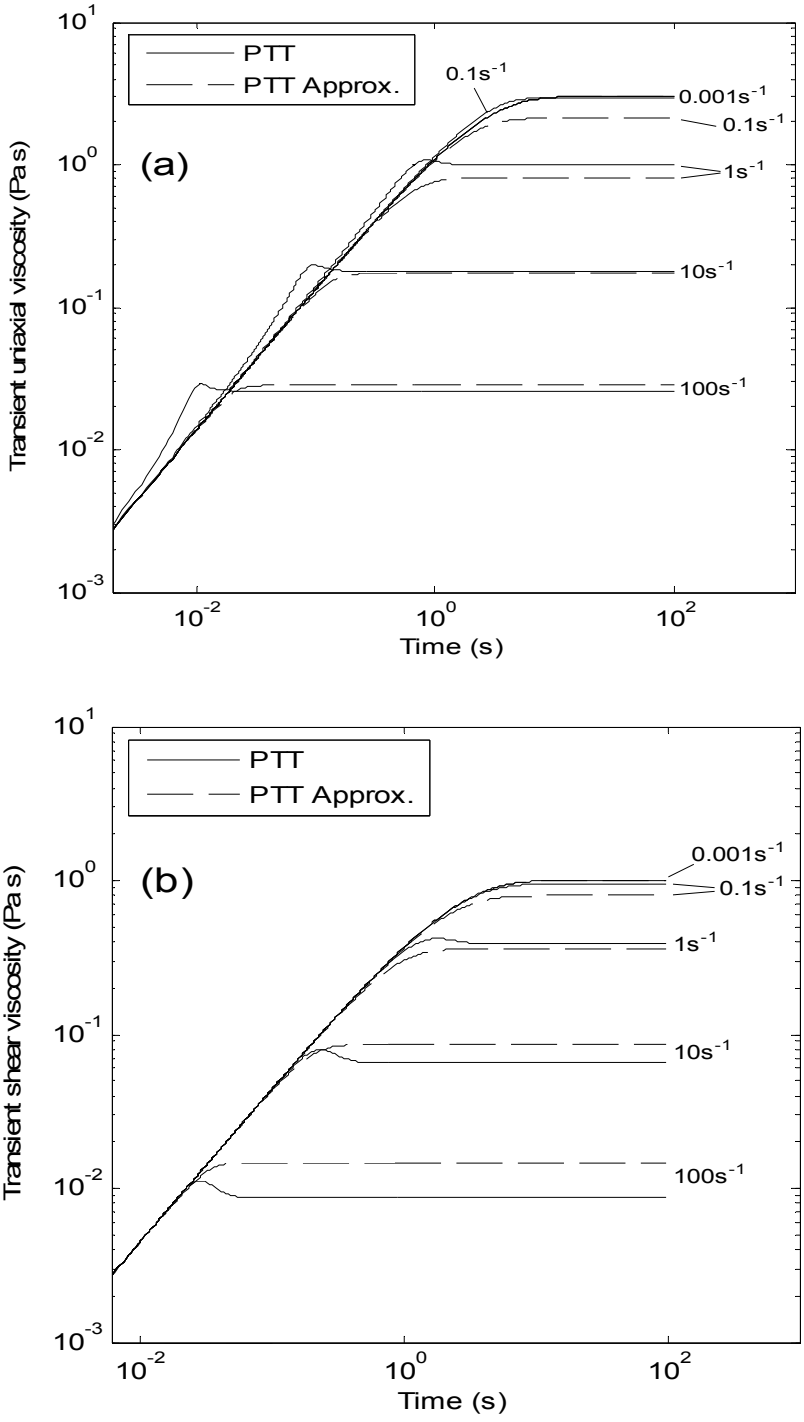

Figure 2 Transient uniaxial viscosities (a) and shear viscosities (b) for the full PTT model and the PTT approximation model at a range of extension and shear rates.

Considering first the uniaxial response in Figure 2(a), the models coincide (to graphical scale) at a rate of $0.001s^{-1}$. At higher rates the full PTT model shows stress overshoots (as are generally seen in viscoelastic materials) and rises above the linear viscoelastic extensional curve before settling to steady-state values (the linear viscoelastic extensional curve is closely represented by the curve at $0.001s^{-1}$, and reaches a steady-state value equal to $3\eta_0$ for both models). The PTT approximation doesn't give stress overshoots, and settles to its steady-state values more directly. The rates of strain softening are also different. At an extensional rate of $0.1s^{-1}$ the full PTT model is seen to rise slightly above the linear viscoelastic extensional curve before settling to a level that is marginally below $3\eta_0$, whereas the PTT approximation shows appreciable shear thinning at this rate. By a rate of $10s^{-1}$ the shear thinning levels of the two models are approximately equal, and the full PTT shows the greater shear thinning by an extensional rate of $100s^{-1}$. Significantly the PTT approximation never rises above the linear viscoelastic extensional curve, and follows a strain softening behaviour more typical of a power law model (or the Doi-Edwards model). Differences are more pronounced when using much lower values of ε as the full PTT can give steady-state uniaxial viscosities which are higher than $3\eta_0$ at some rates. The uniaxial viscosity of the PTT approximation, on the other hand, reaches a maximum value of $3\eta_0$ at all rates when ε is set to zero. Figure 2(b) shows the shear viscosities; both the PTT and PTT approximation give a steady-state viscosity equal to η_0 at very low rates (represented by the curve at $0.001s^{-1}$), and show shear-thinning at higher rates. In shear there are similar rate dependencies to those in uniaxial extension with shear-thinning being more pronounced in the PTT approximation at a shear rate $0.1s^{-1}$, but more pronounced in the full PTT at a rate of $10s^{-1}$ and above.

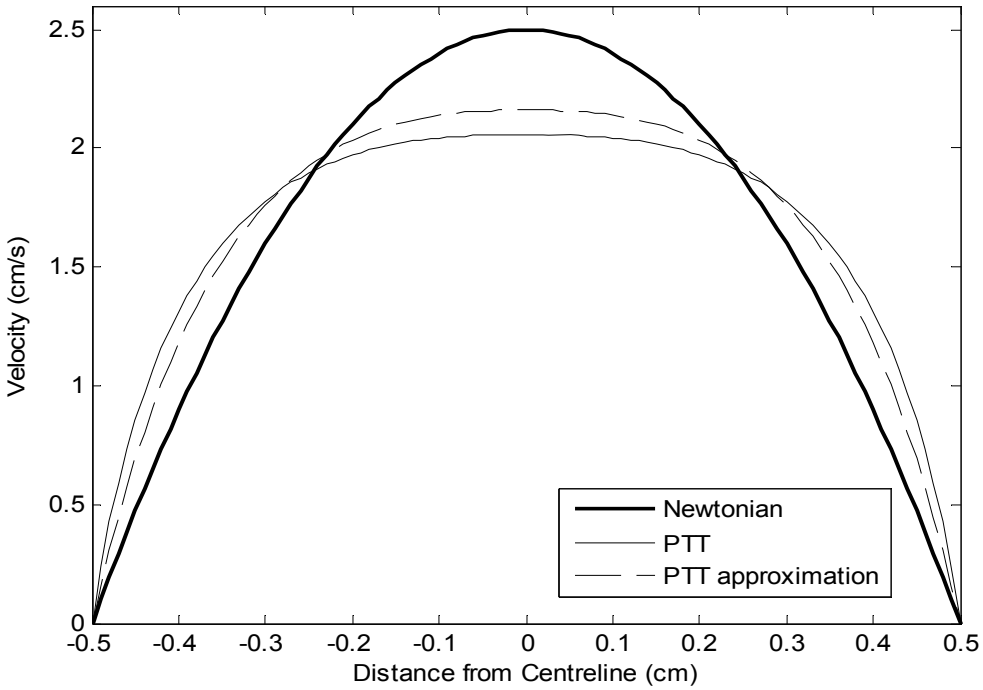

Figure 3 Hele-Shaw flow profiles for the PTT approximation model, the full PTT model and a Newtonian fluid at an apparent shear rate of $10s^{-1}$.

Figure 3 shows the behaviour of the PTT approximation model and the full PTT model in a 1D Hele-Shaw flow, along with a Newtonian fluid as a reference. The flow is between parallel plates which are separated by 1cm, and the PTT based models use the same parameters that are used in Figure 2. The flow profiles were computed using the finite difference method [22] on a 1D grid with 0.01cm spacing. For all curves the apparent shear rate is $10s^{-1}$. The lower shear-thinning of the PTT approximation at high shear rates (compared with the PTT model) can be seen as a less steep velocity gradient near the walls, with higher velocity values in the centre as a consequence of this. Overall the changes from the Newtonian flow profile are qualitatively similar.

There are significant differences in behaviour between the full PTT and the approximation in both shear and extension, however the PTT approximation retains the key aspect of gradual stress growth from the full PTT (associated with elasticity) and also gives stress relaxation (demonstrated later in this work). The approximation also gives a rate dependence that is comparable to 'power-law' or Doi-Edwards models. The approximation model brings these characteristics into simulation at a computational cost that is only slightly greater than that of a time-stepping 'power law' model.

3 Incorporating the Pseudo-Concentration Method

The pseudo-concentration method can be used for simulation of the GAIM process to track the progress of a polymer and a gas phase in a flow. This involves a time-stepping procedure where the polymer "concentration" is convected with the flow. The pseudo-concentration method uses a scheme whereby polymer has a concentration value, c, of 1 and a (low-rate) shear viscosity of η_{0p} and the driving fluid (gas in GAIM) has a concentration value of 0 and a viscosity of μ_g. The method also allows areas of polymer-gas interface $(0 < c < 1)$. The concentration parameter, c, is transported according to

$$\frac{Dc}{Dt} = \frac{\partial c}{\partial t} + \mathbf{u} \cdot \nabla c = 0 \quad , \qquad (5)$$

where $\mathbf{u}$ is the velocity vector. Upon completing a time-step, the value of *c* at any point in the flow field can be used to calculate local values of material dependent properties, often using a linear interpolation method to interpolate between polymer values and gas values [1]. In this implementation the local value of low-rate shear viscosity, η_{0c}, is calculated using such an interpolation method, according to

$$\eta_{0c} = c\,\eta_{0p} + (1-c)\,\mu_g \quad . \qquad (6)$$

The interpolation ensures that in a purely polymer area (where $c = 1$) the local low-rate shear viscosity, η_{0c}, is equal to the polymer low-rate shear viscosity (η_{0p}), and in a purely gas region (where $c = 0$) η_{0c} is equal to the gas viscosity (μ_g); in regions of polymer-gas

interface (where $0 < c < 1$) Eq.6 gives a continuous interpolation between polymer low-rate viscosity and gas viscosity.

The stress transport equation (Eq.2) is written in terms of a low-rate shear viscosity of a polymer (η_0) and a polymer time constant (λ). Rewriting Eq. (2) explicitly in terms of the local (concentration dependent) viscosity, η_{0c}, and a local (concentration dependent) time constant, λ_c, gives

$$\lambda_c \frac{D\overline{\tau}}{Dt} + \overline{\tau} \exp\left(\frac{\varepsilon \lambda_c \overline{\tau}}{\eta_{0c}} \right) = \eta_{0c} \overline{\dot{\gamma}} \ . \qquad (7)$$

In this equation the low rate viscosity of a polymer (η_0) has been replaced by the concentration dependent low rate viscosity (η_{0c}) which in a flow is the *local* low-rate shear viscosity. The time constant (λ_c) is similarly interpolated such that it is equal to the polymer time constant in polymer, and is equal to zero in gas (as gas is Newtonian). This gives a model which in areas where $c = 1$ will return the polymer stress (and thus the polymer viscosity using Eq.4), and will return the gas stress and thus gas viscosity in areas where $c = 0$; it will also return interpolated stress and viscosity in polymer-gas interface areas $(0 < c < 1)$. To moderate the very large dynamic range between polymer and gas viscosities, it is normal to use a gas viscosity value of around $\mu_g = 10^{-4} \eta_{0p}$; this value is used in this work.

As indicated above, the time constant, λ_c, in Eq. 7 is dependent on the local material and thus the concentration value. In this work an interpolation (similar to that used for low-rate viscosity) is used for the time-constant

$$\lambda_c = c\,\lambda_p + (1-c)\,\lambda_g \,, \qquad (8)$$

where λ_p is the characteristic time constant of the polymer, and λ_g is the characteristic time constant of the gas. As previously mentioned, gas (being Newtonian) will have a time constant of zero seconds, hence Eq. 8 actually reduces to $\lambda_c = c\,\lambda_p$. The interpolated value of λ_c is used (along with η_{0c}) in the stress evolution equation (Eq. 7). In a gas (where c = 0) Eqs. 8 and 6 give $\lambda_c = 0$ and $\eta_{0c} = \mu_g$ respectively, and Eq. 7 simplifies to $\overline{\tau} = \mu_g \overline{\dot{\gamma}}$. This gives an apparent viscosity of μ_g (using Eq. 4), as expected for a Newtonian gas.

3.1 Numerical Solution Context

It is valuable at this point to put Eqs. 3 to 8 in the context of a numerical solution to a 2-D or 3-D flow problem. A solution requires that initial concentration values are set everywhere (for example to *c=1*, for an area that is initially full of polymer) and also requires that there is an initial Newtonian flow solution to start the process (a single time step according to initial

boundary conditions is appropriate). Suitable boundary conditions are also necessary for *c,* as covered later. From this starting point a time-stepping procedure follows in the following order:

a) the concentration equation (Eq.5) is time-stepped to update the *c* field;

b) values of η_{0c} and λ_c are then calculated at all required points according to Eqs. 6 and 8 respectively;

c) these values of η_{0c} and λ_c are inserted in Eq.7 and the stress field is time-stepped;

d) the local values of apparent viscosity (μ_a) at all required points are then calculated using the updated stress values and Eq.4;

e) these local apparent viscosities are then used in the next time-step of a Newtonian flow solver, according to

$$\rho \frac{D\mathbf{u}}{Dt} = \nabla \cdot \left[\mu_a \left(\mathbf{L} + \mathbf{L}^{\mathrm{T}} \right) - \mathbf{I}p \right] \tag{9}$$

where ρ is density, and μ_a is apparent viscosity; $\mathbf{u}$ is the velocity vector, p is pressure and $\mathbf{L}$ is the velocity gradient tensor given by $L_{ij} = \partial u_i / \partial x_j$. The continuity equation $\nabla \cdot \mathbf{u} = 0$ must also be imposed.

At the end of steps a) – e) all field values have completed one time-step, and the next time-step can continue from point a) .

4 Finite Element Simulation

The PTT Approximation model was implemented using 8 noded 3D “brick” elements with linear interpolation. Linear elements are helpful in pseudo-concentration simulations due to the necessity of “clipping” calculated nodal values of c to be between 0.0 and 1.0 [2].

The concentration transport equation (Eq.5), stress transport equation (Eq.7) and velocity and pressure equations (Eq.9 along with the continuity equation $\nabla \cdot \mathbf{u} = 0$) were discretised using the Galerkin method [22]. Backwards time-differencing and upwinding were used to maintain stability in the highly convective stress and concentration transport equations. The upwinding method used was that of Ref. [23] which provides stabilising diffusion in the direction of flow. The velocity and pressure equations (Eq.9) were used with the convective terms neglected due to the low Reynolds numbers involved, and no upwinding was needed for these equations. Pressure p was interpolated using one order lower interpolation functions than used for the velocity components, as is common for finite element implementations of flow equations.

The simulation of a given problem begins by initialising concentration values to 0 (for gas) or 1 (for polymer). An initial Newtonian time-step (using the prescribed boundary conditions) is

needed to start the process. An outline of the time-stepping process is given in the previous section. Details of a single time-step are given in the following.

The concentration value c was advanced one time-step from a solution of Eq.5. Having obtained nodal values of c, "clipping" is normal (after each time-step) in the pseudo-concentration method [1]. The values of c that are higher than a threshold value (normally 0.5) are raised to 1.0, and values that are lower than 0.5 are reduced to 0.0. This is performed everywhere except for nodes belonging to elements which contain the contour of $c = 0.5$. Such elements are easily identified (if they use linear interpolation) as they will contain at least one node with a c value over 0.5 and at least one node below 0.5. If this clipping procedure is neglected then time-stepping causes values of c outside the meaningful range of 0 to 1 (arising principally from attempting to model the discontinuous polymer-gas interface using a finite element with finite interpolation).

With the nodal values of c known, values can be interpolated to the element's Gauss points using standard finite element interpolation and values of η_{0c} and λ_c can be calculated at a Gauss point using Eqs. (6) and (8). These values are then used in a time-step computation of Eq. 7 to update $\bar{\tau}$ at all nodes.

With updated values of $\bar{\tau}$ available at all nodes, values of $\bar{\tau}$ can then be evaluated at Gauss points, and divided by the local deformation rate $\dot{\bar{\gamma}}$ to give an apparent viscosity, μ_a, according to Eq. 4. It was found that near to the polymer-gas interface it was possible for the computed values of μ_a to be below those of the gas viscosity, μ_g, or even slightly negative; this again appears to be a consequence of simulating a discontinuous polymer-gas interface using finite elements of finite size and interpolation. Problems of zero viscosity could also occur in creeping flows or reversing flows. To keep the values of viscosity physically reasonable a minimum value of apparent viscosity equal to μ_g ($\mu_g = 10^{-4}\eta_{0p}$) was permitted. There is also the potential for Eq.4 to return a large or infinite viscosity if the shear is at (or near) zero at a point so a top limit of $\mu_a = 10^4 \eta_{0p}$ was also enforced to avoid the potential for singular matrices. The centreline in pipe flows has zero stress and shear giving the potential for such unphysical values of viscosity; this problem was effectively avoided in the current simulations because the viscosities are evaluated at the element Gauss points, which are away from the centreline. In general applications it would be advisable to apply limits to μ_a, for example $10^{-4}\eta_{0p} \le \mu_a \le 10^4 \eta_{0p}$.

With apparent viscosity available at all Gauss points, velocity and pressure fields can then be updated in a single time-step of the Newtonian flow equation (Eq.9).

In simulations using the pseudo-concentration method the limit imposed by the Courant criterion ("$U\Delta t < \Delta x$" where Δt is the simulation time-step) must be exceeded by a considerable margin, as pointed out by Haagh et al [1]. Following experiment the criterion $U\Delta t \approx \Delta x/10$ was found to be appropriate to simulations such that the flow did not cross more than 1/10th of an element in a single time-step. Without this limitation the polymer-gas

interface can advance without due regard to the stress gradients in front of it. The effect of too large a time-step is shown in the convergence tests later in this work.

Boundary conditions were used for velocity components and for concentration value, c. Velocity boundary conditions were the standard “non-slip” wall condition where polymer is present at the wall, but the boundary conditions are not imposed if gas is present at the wall. This avoids the problem of corners into which advancing polymer cannot reach and has been shown to give “fountain flow” [2]. Boundary conditions for concentration value need to be set where a flow of gas or polymer enters the problem. If the flow is polymer, then the concentration value is set to 1; if it is gas then the concentration value is set to 0.

As mentioned earlier in the section, initial conditions are necessary for the concentration value. The current simulations are all for a cylinder that is initially filled with viscoelastic material in an initially unstressed state, hence an initial concentration value of 1.0 was used.

5 Results

There are a number of reported studies of gas penetration of viscoelastic fluids, some containing apparently contradictory results. The primary property studied is the *fractional coverage*, m, or the *residual wall thickness,* RWT, left behind after a gas bubble has penetrated. The fractional coverage for a circular cross-section is given by

$$m = \frac{R_0^{\,2} - R_b^{\,2}}{R_0^{\,2}}, \tag{10}$$

where R_0 is the radius of a cylindrical tube, initially filled with viscoelastic fluid and R_b is the radius of the penetrating gas bubble. Huzyak and Koelling [24] performed an experimental study of two viscoelastic Boger fluids based on polybutene. Their work showed a large rise in fractional coverage of the viscoelastic fluid as flow rates (and so the the *Deborah number*) increased. This rise was of the order of 30%. The definition of the Deborah Number used in that work was

$$De_1 = \lambda \dot{\gamma}_w, \tag{11}$$

where λ is the characteristic time constant of the viscoelastic fluid and $\dot{\gamma}_w$ is the wall apparent shear rate. The subscript ‘1’ is used on De since an alternative definition will be needed to compare with other published experimental results.

Simulations by Dimakopoulos and Tsamopoulos using a shear dependent PTT fluid gave some increase in fractional coverage [18] with Deborah Number , whereas simulations by Rasmussen and Eriksson using The Molecular Stress Function (MSF) model gave a general fall in fractional coverage as Deborah Number rose; the latter results were supported by experimental results for a rate dependent linear polymer. The application of the PTT Approximation to the same experimental data is now investigated.

5.1 Comparison with Experimental results for a Boger Fluid

Experimental results for a Boger fluid are given by Huzyak and Koelling [24]. A cylindrical tube was initially filled with viscoelastic fluid and gas injected from one end to leave a

residual coating around the tube radius, from which the fractional coverage was measured. Experiment was complicated by the presence of surface tension in the flows, hence the effects of Capillary Number on fractional coverage were reduced by presenting results for m/m_N against Deborah Number, where m is the fractional coverage for a viscoelastic flow and m_N is the fractional coverage for a Newtonian flow with the same Capillary Number.

With the aim of simulating the flow with the PTT approximation model and using a single characteristic time constant, the relaxation spectrum given by Huzyak and Koelling was used to produce a single representative time constant, $\bar{\lambda}$, for the fluid using the weighted average

$$\bar{\lambda} = \frac{\sum_k \mu_k \lambda_k}{\sum_k \mu_k} \quad . \tag{12}$$

For their data given for the B-100 viscoelastic fluid [24] the value of the time constant is 0.37 sec, and this value was used in the current simulations. It is to be noted that the actual value used for $\bar{\lambda}$ is not critical for simulations of a Boger fluid for which results against De_1 are required, this is because De_1 is proportional to the time constant. As it is a Boger fluid the parameter ε was set to zero to give no shear thinning. The low-rate shear viscosity of the B-100 fluid was used ($\eta_{0p} = 10.4\,Pa\,s$). For the 3D simulation code being used a mesh was constructed using 8-noded "brick" elements which used 2 planes of symmetry. The outer surfaces of the mesh are shown in Fig. 4. The meshed area was 15 pipe radii long to allow a constant residual cross-section to develop (up to certain limits). The mesh contains 18000 elements and 20412 nodes.

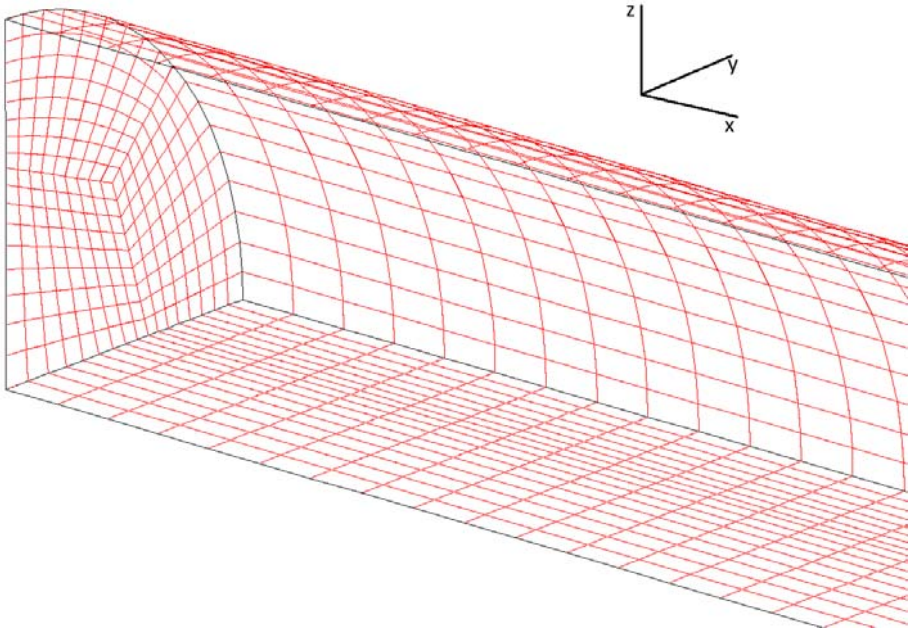

Figure 4 Outer surfaces of the mesh used for simulation (front surface omitted for clarity).

The simulations began with the tube initially full of viscoelastic fluid (c=1), with a parabolic flow of gas being injected from one end (the injected fluid is set as gas by applying c=0 as a boundary condition at the inlet). The stress evolution equation (Eq. 7) doesn't require any enforced inlet or wall boundary conditions. Fig. 5 summarises the boundary conditions, and shows solid contours of concentration, c, to illustrate the progress of injected gas along the pipe.

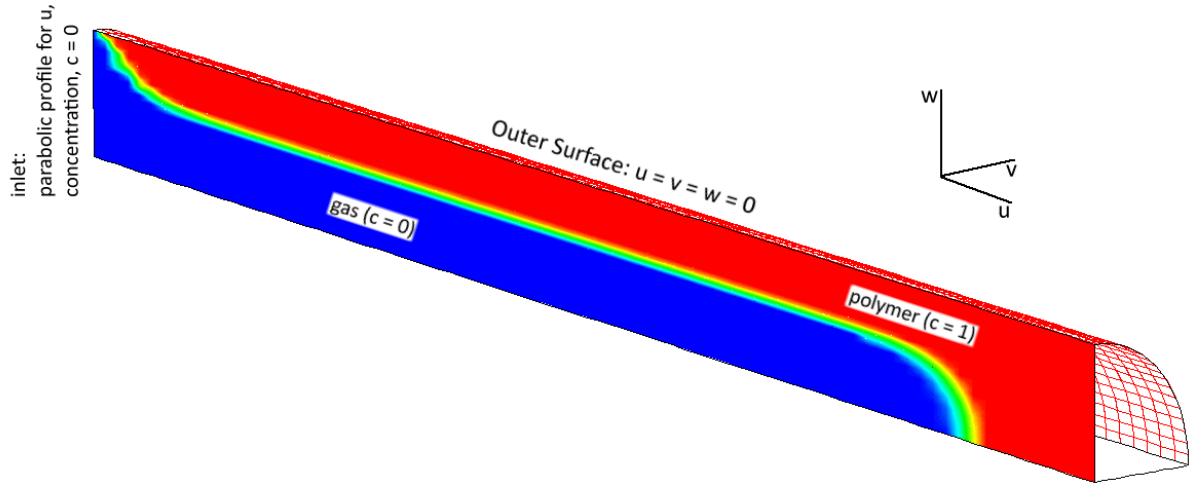

Figure 5 Applied boundary conditions (symmetry boundary conditions not shown), u, v and w are the velocity components in the x, y and z directions respectively. Solid contours of concentration in x-z plane are shown to illustrate gas flow.

The apparent wall shear rate, $\dot{\gamma}_w$, used to calculate De_1 was calculated directly from the form of the applied parabolic flow. Simulation continued until after the gas bubble reached the far end of the mesh, and fractional coverage was determined by measuring R_b the radius of the contour of concentration, $c = 0.5$. Measurements were made in the x-z plane (axes indicated in Fig. 4) at a point three quarters of the way along the pipe from the inlet. This position gave sufficient distance for a fully developed region to appear (up to certain limits) and avoided effects from the pipe exit.

Deborah number could be increased by increasing the inlet flow rate; at each increase the time-step used was decreased to maintain the criterion "$U\,\Delta t \approx \Delta x/10$", as discussed in Section 4 (and studied further in Section 7). It was found that as the Deborah number increased a longer distance along the pipe was required for a fully developed region to occur. Beyond a Deborah number of approximately 20 no fully developed region could be found for the Boger fluid within the length of pipe simulated.

Fig. 6 compares the experimental results of Huzyak and Koelling (for their fluids named B-25 and B-100) with the corresponding results for the simulation.

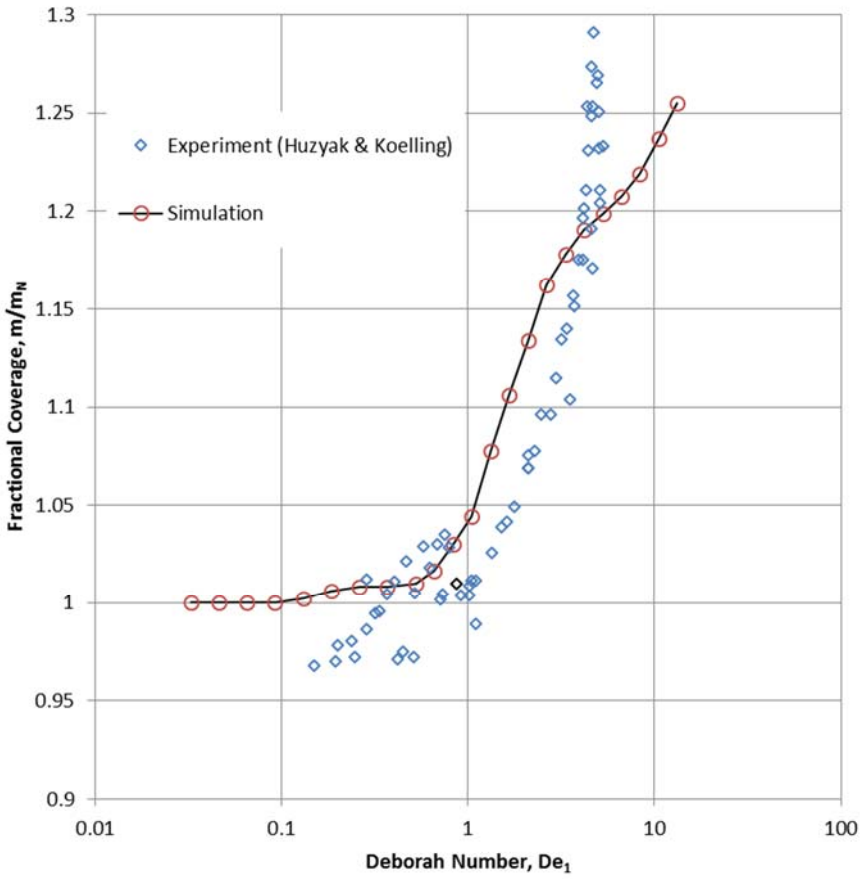

Figure 6 Comparison of Experimental results from Ref. [24] with results simulated using the PTT Approximation model

The experimental results for the two fluids are plotted together, since the current simulation will give identical results for Boger fluids of different time constant when dimensionless results are plotted as a function of De_1. The simulation is seen to predict a sharp rise in fractional coverage from a Deborah number of approximately 1, in good agreement with the experimental data. As the Deborah Number reduces the simulation tends towards a Newtonian solution ($m = 0.61$ in our simulations), which is to be expected for a viscoelastic constitutive equation. The experimental data shows a drop below Newtonian levels at low Deborah numbers, although this may be only a second order effect of the finite Capillary numbers. The last data point is given tentatively since, upon leaving the simulation to run after the bubble had reached the end, instabilities developed in the simulated interface resulting in the loss of the fully developed region. This may be due to the large levels of "elasticity" at such high Deborah numbers being emulated by the model.

Overall the level of agreement is remarkable considering both the approximation in the model, and the use of no arbitrarily chosen parameters (both ε and λ are set by the fluid as described above), and the author is not aware of a comparable simulation match to this experimental data.

Fig. 7 shows corresponding plots of the c = 0.5 contour and the scalar stress, $\overline{\tau}$, with the bubble front fully-developed, approximately half-way along the cylinder. Part a) of this figure superimposes the velocity vectors showing an approximately parabolic flow in the gas, which diverges as it approaches the polymer interface (c=0.5); the polymer and gas areas are also indicated. The right hand end of part b) shows an approximately constant distance between contour lines indicating an approximately linear rise in the stress in the polymer away from the centreline. This is as expected for a flow approaching steady-state laminar flow. The contours dip towards the front of the advancing bubble showing a rise of stress in this region. The area above the gas region shows gradual stress relaxation due to the time since the polymer was deforming appreciably. The evolution of the bubble front along the pipe is shown in Fig. 8.

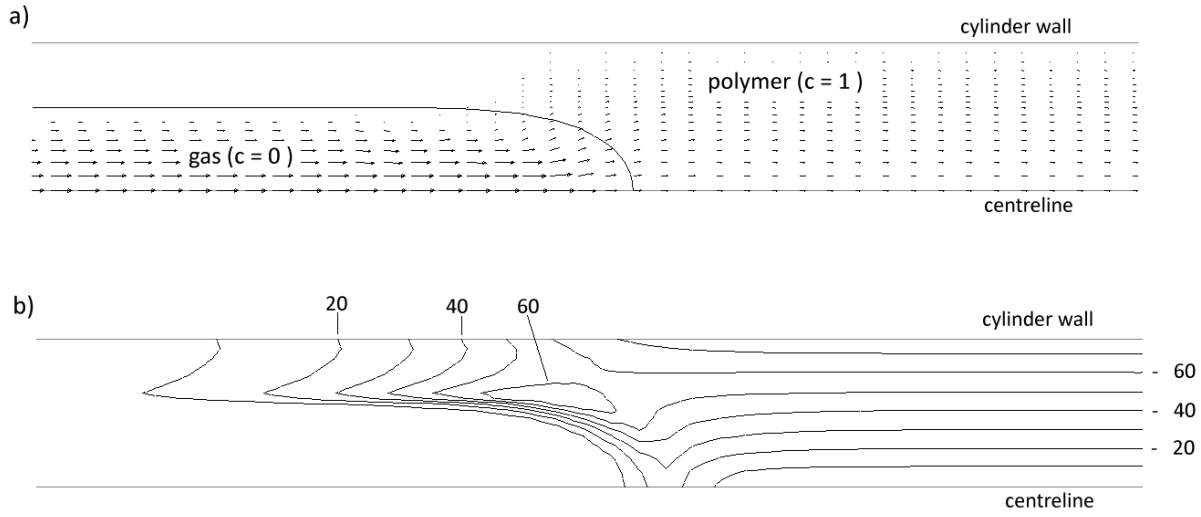

Figure 7 Concentration, c, and scalar stress, $\overline{\tau}$, in a radial cross-section at a Deborah number (De_1) of 2.09 (relative fractional coverage, m / m_N = 1.13). a) Contour of c = 0.5 and velocity vectors around the bubble front. b) Corresponding contours of scalar stress; numeric labels give the stress in Pa.

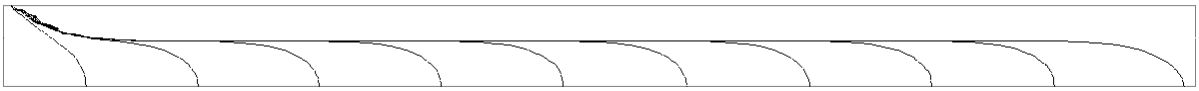

Figure 8 Showing the evolution of the bubble in a radial cross-section as time progresses. The Deborah number is 2.09 and the contours of c = 0.5 are shown at time intervals of 0.354s.

5.2 Comparison with experiments for a shear-thinning viscoelastic fluid

Simulations of viscoelastic fluids that include shear-thinning have produced qualitatively different results from different simulations. Dimakopoulous & Tsamaopoulos [18] simulated viscoelastic gas penetration using a PTT model and found a slight increase in wall thickness

with increasing Deborah number. Rasmussen and Eriksson simulated a linear polymer flow using a molecular stress function model [15] and found a marked decrease in wall thickness with Deborah number, which corresponded to their experimental results.

The experimental results given by Rasmussen and Eriksson were for polystyrene, and details of the storage and loss moduli (G' and G'') were given, along with the version of the Deborah number that they employed, De_2, where

$$De_2 = \frac{G'}{G''}\left[1+\left(\frac{G'}{G''}\right)^2\right]^{0.2}. \tag{13}$$

The version De_2 arises from substituting the Cox-Merz rule for shear viscosity and Laun's rule for first normal stress difference into the fundamental definition of the Deborah number [15]. For a given flow G' and G'' are evaluated at an angular frequency ω, given by

$$\omega = \frac{U}{R_0}, \tag{14}$$

where U is calculated from the total length of the polymer rod divided by the total time for the gas to penetrate the length. R_0 is the outer radius of the pipe [15]. Rasmussen and Eriksson gave the G' and G'' values for 150 °C graphically, whereas the viscoelastic gas penetration measurements are performed at 170°C. In order to use their rheometric values readily, the graphical data points were extracted using an optical means and these fitted to polynomials, giving the following relationships:

$$\log_{10} G' = 4.805 + 0.3316\ell - 8.079\times10^{-2}\ell^2 + 1.903\times10^{-2}\ell^3,$$

$$\log_{10} G'' = 4.542 + 1.833\times10^{-1}\ell - 3.965\times10^{-2}\ell^2 + 1.616\times10^{-2}\ell^3, \tag{15}$$

where $\ell = \log_{10}(\omega)$. The curve fits are shown in comparison to the extracted 150 °C data in Fig. 9.

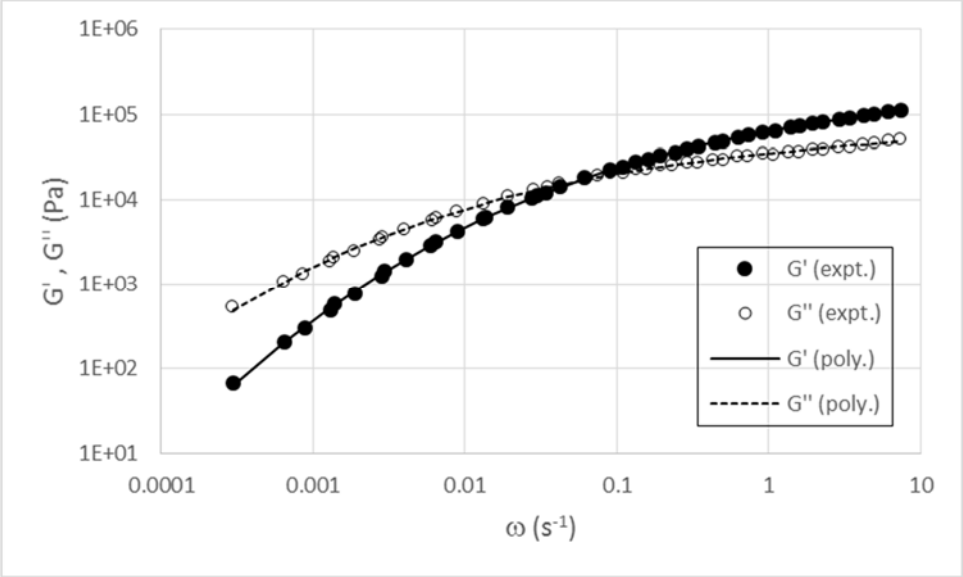

Figure 9 Comparison between experimental data (Rasmussen and Eriksson) and polynomial curves.

Rasmussen and Eriksson fitted the G' and G'' data to a Baumgaertel, Schausberger and Winter (BSW) memory function model for use in a linear Molecular Strain Function (MSF) constitutive model. To use the data in a PTT model it is necessary to fit to a relaxation constant (for λ), or Maxwell relaxation spectrum.

To generate the relaxation spectra the method described by Haghtalab and Sodeifian [25] was adopted to fit to a range of relaxation rates λ_i and relaxation moduli g_i. This method requires that a range of relaxation time constants, λ_i, are selected and a set of linear equations is constructed using the equations

$$G'(\omega)=\sum_{i=1}^{N} g_i \frac{\omega^2 {\lambda_i}^2}{1+\omega^2 {\lambda_i}^2} \quad , \tag{16}$$

and $$G''(\omega)=\sum_{i=1}^{N} g_i \frac{\omega \lambda_i}{1+\omega^2 {\lambda_i}^2} , \tag{17}$$

at many different values of ω. This set of equations can then be solved for the values of g_i using a least squares method. The spectrum obtained for the 150 °C data is given below.

i	λ_i (s, at 150°C)	g_i (Pa)
1	0.1000	7.911×10^4
2	0.3728	2.232×10^4
3	1.389	3.015×10^4
4	5.179	2.004×10^4
5	19.31	1.245×10^4
6	71.97	6.920×10^3
7	268.3	1.477×10^3
8	1000.0	5.132×10^2

Table 1 Relaxation spectra obtained from G' and G'' data by Rasmussen and Eriksson [15]

The effectiveness of the method can be seen from comparing the extracted data values with the values produced by using the spectrum of λ_i, g_i values in Eqs. (16) and (17) above. This is shown in Fig. 10.

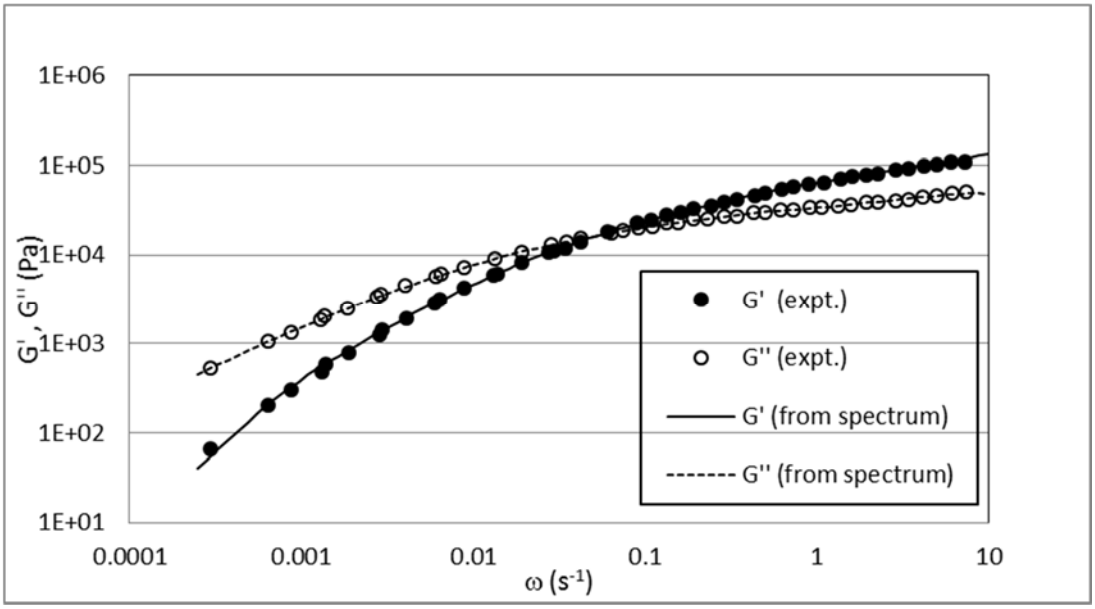

Figure 10 Comparison between experimental data [15] and the relaxation spectrum values

A sensible measure of a representative single value for a relaxation constant, $\overline{\lambda}$, can be obtained from a weighted average of time constants, using viscosity contribution as the weighting factor – the formula is shown in Eq. (12). This gives a value for $\overline{\lambda}$ of 365.1s at 150°C. After time-temperature shifting to 170°C (the temperature at which complex gas penetration measurements are performed) this value is modified to 25.4 seconds.

An alternative method of finding a single relaxation constant was developed. Trial values of $\overline{\lambda}$ were used as the single value of "λ_i" and a value of "g_i" found using the method outlined

above. The predictions of the resulting fit were then compared with the experimental values, and a residual fractional error, $\bar{e}$, calculated where

$$\bar{e} = \sum \left(\left| \frac{G'(\omega) - \overline{G'}(\omega)}{G'(\omega)} \right| + \left| \frac{G''(\omega) - \overline{G''}(\omega)}{G''(\omega)} \right| \right) , \tag{18}$$

where $G'(\omega)$ and $G''(\omega)$ are the experimental storage and loss moduli, and $\overline{G'}(\omega)$ and $\overline{G''}(\omega)$ are the equivalent values predicted from the single value of $\bar{\lambda}$. This was repeated for $\bar{\lambda}$ ranging from 10^{-1} seconds to 10^{3} seconds, in a large number of logarithmically even steps. This method gave a best value for $\bar{\lambda}$ of 31.6 seconds. After time-temperate shifting to 170°C this value is modified to 2.20 seconds. Thus there are 2 candidate values for $\bar{\lambda}$ at 170°C, each produced by a method which may be considered 'reasonable', but widely separated at 2.20 seconds and 25.4 seconds respectively. These values are now assessed against transient behaviour before proceeding to simulation.

Rasmussen and Eriksson performed simulations using the Linear Molecular Stress Function (LMSF) [26] which gives the extra-stress, $\boldsymbol{\tau}(t)$ in a linear polymer melt as

$$\boldsymbol{\tau}(t) = \int_{-\infty}^{t} m(t-t')\, \mathbf{S}_{\mathbf{MSF}}(t')\, dt' \tag{19}$$

where $\mathbf{S}_{\mathbf{MSF}}$ is the strain measure, and $m(t-t')$ is the memory function between time t' in the past, and the current time *t*. The strain measure of the Molecular Stress Function is given by $\mathbf{S}_{\mathbf{MSF}} = f^2 \mathbf{S}_{\mathbf{DE}}$, where $\mathbf{S}_{\mathbf{DE}}$ is the Doi-Edwards strain function, and

$$f^2 = 1 + \left({f_{\max}}^2 - 1 \right) \left[1 + \exp\left(- \frac{e^{\langle \ln u' \rangle} - 1}{\left({f_{\max}}^2 - 1 \right)} \right) \right], \tag{20}$$

where $\langle \ln u' \rangle$ is the spherical average of the natural logarithm of deformed segment lengths (see [26]). The model has only one adjustable parameter, $f_{\max}$, which sets the maximum stretch value. Rasmussen and Eriksson obtained closest fit to strain-hardening rheological data with ${f^2}_{\max}$ set to 5. A value of $f_{\max}$ = 1 was used as a lower bound for simulation and gave a good fit to experimental fractional coverage data. The PTT approximation will not give the strong strain hardening needed to match the polystyrene's uniaxial extension data well (a value of $\varepsilon = 0$ only gives a linear viscoelastic response), however the LMSF simulation results with $f_{\max} = 1$ are equivalent to the Doi-Edwards model. This provides a means to select "matching" values of ε for Eq. (2):- the full relaxation spectrum in Table 1 can be used to give predictions of response using a Doi-Edwards model, and these compared with the output of the PTT approximation model (given by Eq. (2)) to obtain best values of ε .

Figs. 11 and 12 show comparison of uniaxial transient viscosity for the Doi-Edwards model (using the full spectrum of time constants) and the PTT Approximation, for $\bar{\lambda}$ =2.2 seconds and $\bar{\lambda}$ =25.4 seconds, respectively. The fit for $\bar{\lambda}$ =2.2 seconds was obtained using a value

of ε of 1.3, and the fit for $\overline{\lambda}$ =25.4 seconds was obtained using a value of ε of 0.11. The values of ε were chosen to best match the plateau levels of transient viscosity. The viscosity values rose at earlier times than the Doi-Edwards model when using a time constant of 2.2 seconds, and at later times when using 25.4 seconds. This is a consequence of using a single time constant, as opposed to the spectrum of time constants used in the Doi-Edwards results.

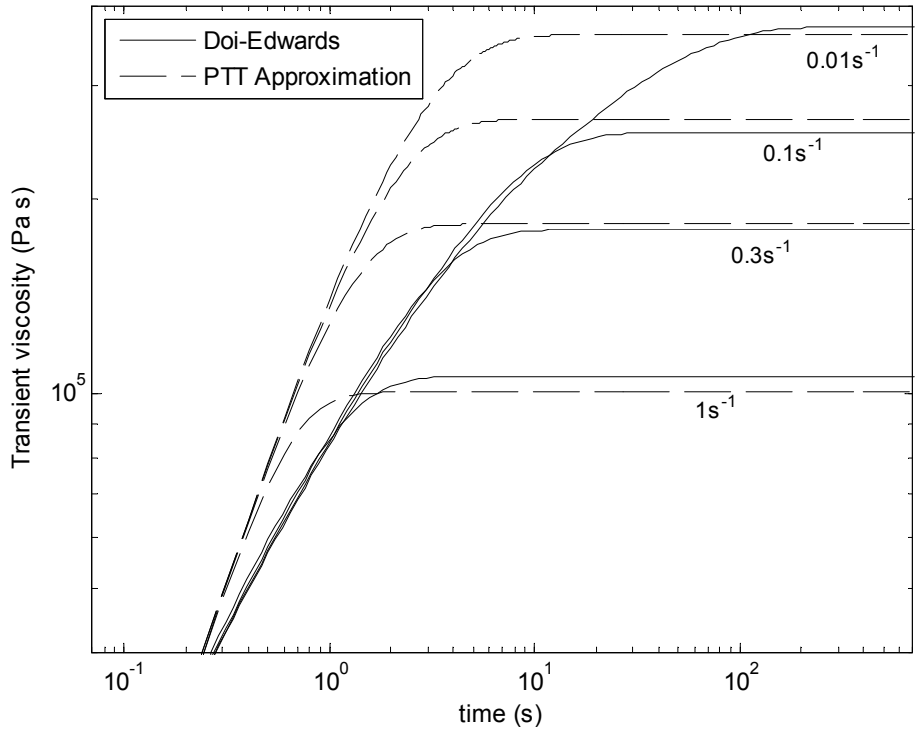

Figure 11 Comparison at 170°C of transient uniaxial viscosity given using the Doi-Edwards model with the full spectrum of relaxation data, and the PTT Approximation with a single time constant of 2.20 seconds.

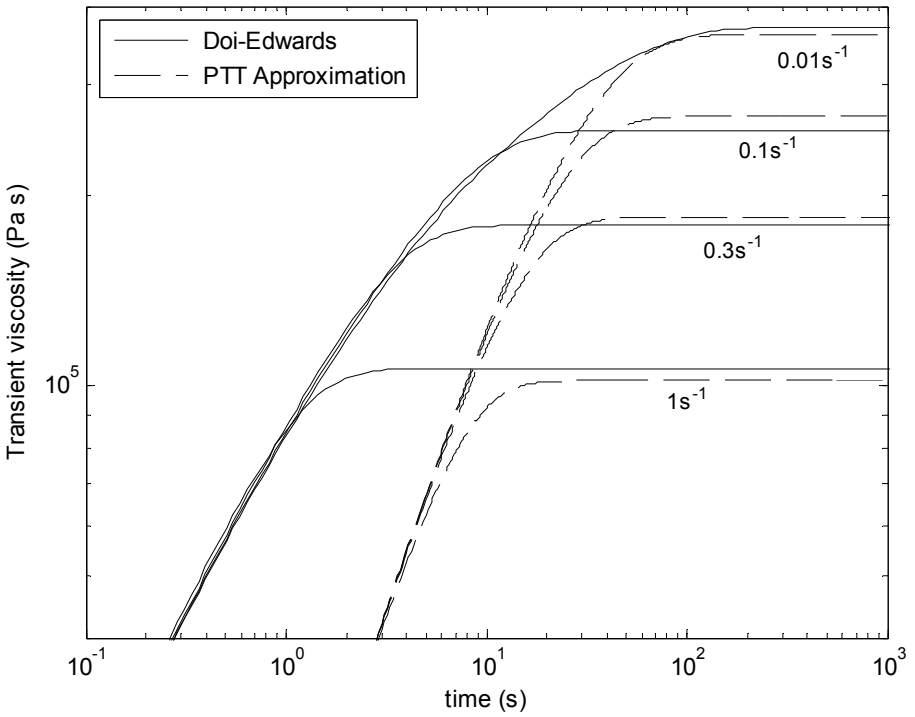

Figure 12 Comparison at 170°C of transient uniaxial viscosity given using the Doi-Edwards model with the full spectrum of relaxation data, and the PTT Approximation with a single time constant of 25.4 seconds.

Simulations were performed for both values of time constant in the manner described in Section 4. Direct comparison with the experimental and simulation data of Rasmussen and Eriksson [15] required finding a common definition of Deborah number. To match the Deborah number used by [15], De_2, the angular frequency, ω, could first be calculated using Eq. (14), then calculating G' and G'' using Eq. (15) and then obtaining De_2 from Eq. (13). However this would be inappropriate for the current simulations as they use single values of λ and so don't well represent the full G' and G'' data. Also the data from ref. [15] doesn't convert exactly to be in terms of De_1. Common ground was found using an approximation based on Newtonian flow profile (as widely used to calculate apparent wall shear rates). The method is as follows: for a given apparent wall shear rate, $\dot{\gamma}_w$, the Newtonian centre velocity, U_{cen} is given by $U_{cen} = \dot{\gamma}_w R_0 / 2$, and so ω is given by $\omega = \dot{\gamma}_w / 2$ using (14); from this corresponding value of De_2 can be calculated using Eqs. (15) and (13) as described earlier in this paragraph. A corresponding value of De_1 can also be calculated at an apparent shear rate, using the mean effective value of time constant obtained from the full viscoelastic spectrum as given by Eq. (12) – this value is 365.1 sec at 150°C as described above. Repeating for a range of apparent wall shear rates means that corresponding values of De_1 and De_2 can be obtained as shown in Fig. 13. Using this relationship the De_2 based data of Rasmussen and Eriksson can be plotted versus De_1 (a significant approximation is involved but it allows a sufficiently qualitative comparison for further progress, as will be seen). Fig. 13 also shows the effect of leaving out data points:

the G' and G'' data points at both highest and lowest values of angular frequency were removed and the fitting procedure repeated giving a modified relationship (through their effect on the coefficient values in in the relationships given in Eq. 15); the difference is slight across the range showing a good level of insensitivity to leaving out end data points.

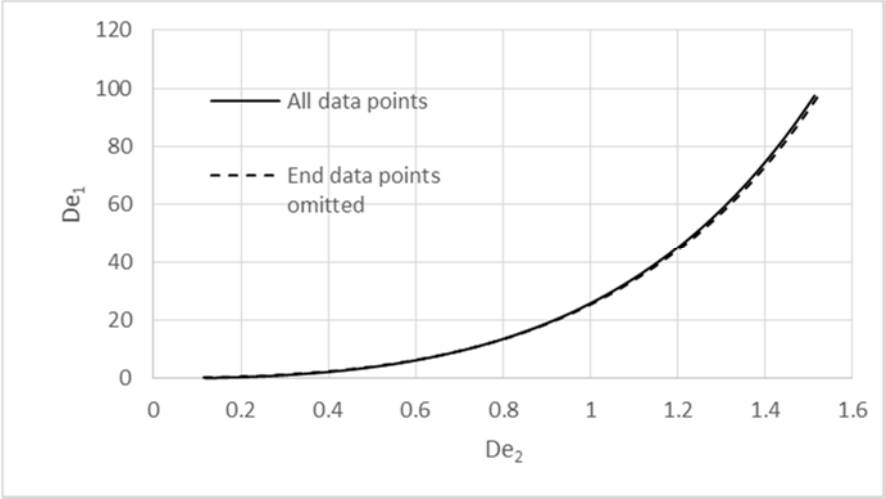

Figure 13 De_1 (Deborah number given by Eq. 11) versus De_2 (Deborah number used by ref.[15])

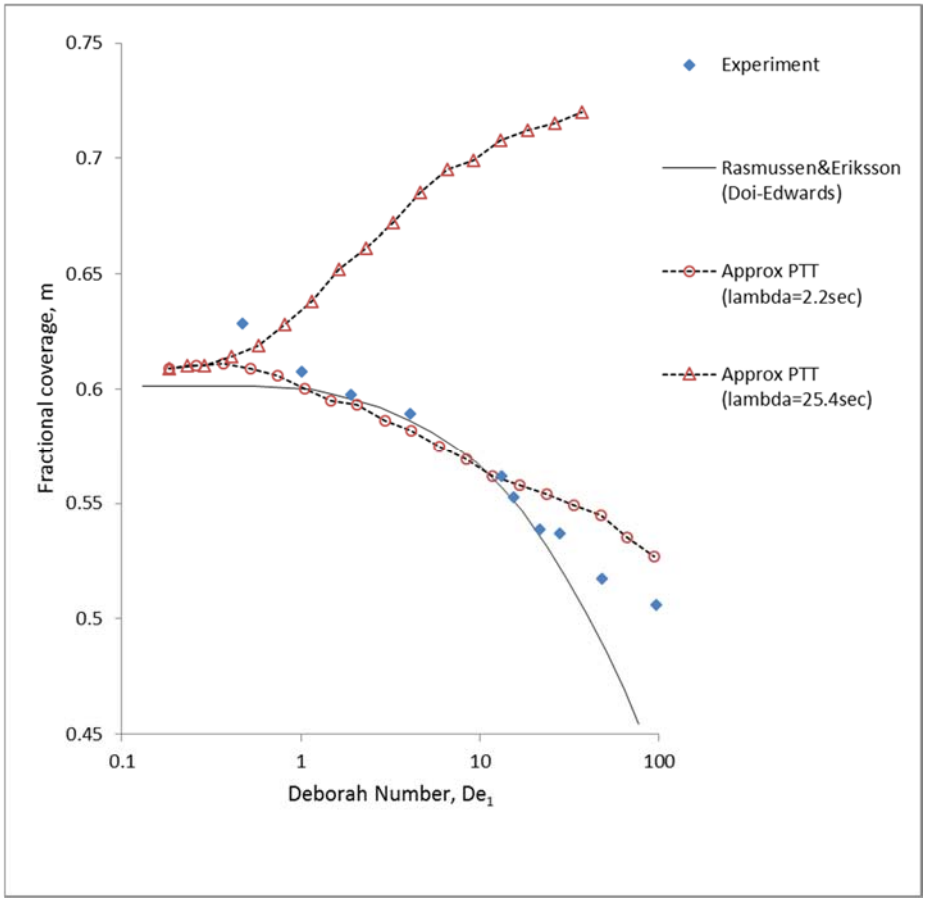

Figure 14 Comparison between single time constant simulations and experimental data and Doi-Edwards based simulation data from ref. [15].

Fig. 14 shows the results when plotted against De_1 using the approximate correspondence of Fig. 13. It can be seen that both the simulation and experimental data of Rasmussen and Eriksson show the fractional coverage reducing with Deborah number - this is in contrast to the Boger fluid where there was a clear increase. The current simulations show that the choice of single time constant is critical: with a time constant of 2.2 seconds the simulations show a drop in fractional coverage with Deborah number, whereas with a time constant of 25.4 seconds the fractional coverage increases. The impression is that the extensional effects seen in the Boger fluid (that tend to cause an increase in fractional coverage) dominate the shear thinning effects when the time constant is long. The match to experimental data from the 2.2 second time constant is qualitatively good. The low Deborah number value for fractional coverage is 0.61 in these simulations, which is slightly higher than the corresponding value of 0.60 given by refs. [15] and [18]; these two references use a Lagrangian (moving mesh) approach, and a key difference between Lagrangian methods and the pseudo-concentration (Eulerian) method is discussed later.

6. Multi-mode PTT Approximation

The results for the shear-thinning fluid suggest that finding the single time constant that gives the best fit to the G' and G'' data gives at least qualitatively good results on a shear thinning viscoelastic fluid. There is room for improvement however as the conversion of data

between different definitions of Deborah number contains approximations. A “multi-mode” model was developed to remove this uncertainty; this happens because the definite value of De_2 can be determined as a multi-mode model naturally uses the full rheometric spectrum (using G' and G'' data). Additionally there is no uncertainty associated with choosing a “best” single time constant.

To generalise Eq. 7 an evolution equation was used for each mode in the relaxation spectrum, i.e.:

$$\lambda_{c,i}\frac{D\overline{\tau}_i}{Dt}+\overline{\tau}_i\exp\left(\frac{\varepsilon\lambda_{c,i}\overline{\tau}_i}{\eta_{0c,i}}\right)=\eta_{0c,i}\overline{\dot{\gamma}} \qquad (21)$$

where $\eta_{0c,i}$ is the low rate viscosity of a single mode, given by $g_i\lambda_i$ for polymer (where c=1) and given by the lower $10^{-4}g_i\lambda_i$ for gas (where c=0), with interpolation similar to that of Eq. (6) for values of c between 0 and 1. $\overline{\tau}_i$ is a measure of the viscoelastic stress of a single mode. A single common value of the rate dependence parameter, ε, is used for all modes here; by analogy to the full PTT model there remains an option to use independent values, ε_i, for each mode. In place of an evolution equation to calculate stress associated with a single time constant there is an evolution equation to calculate the stress associated with each mode. The different modes can be computed sequentially which avoids large bandwidth (and thus large computational time) and is in keeping with producing a time-efficient approximation. Once the stresses from each mode have been calculated they are added to give an overall stress $\overline{\tau}$, where

$$\overline{\tau}=\sum_{i=1}^{i=N}\overline{\tau}_i\ . \qquad (22)$$

From this stress an apparent viscosity, μ_a is produced as in the single mode method, and used for the next time-step of a time-stepping Navier-Stokes type simulation.

An appropriate value for the adjustable parameter, ε, was found by comparing predictions of extensional viscosity with predictions from the Doi-Edwards model using the same relaxation spectrum. The Doi-Edwards model was used for comparison as it gave good results on the problem when used by Rasmussen and Eriksson and it requires no parameters beyond the relaxation spectrum.

Fig. 15 shows the fit obtained using a value for ε of 0.33 which gave the best by-eye fit over the range of extension rates. The multi-mode approximation is seen to follow the overall viscoelastic behaviour appropriately with a tendency to over-predict extensional viscosity at the higher extension rates and under-predict at the lower extension rates.

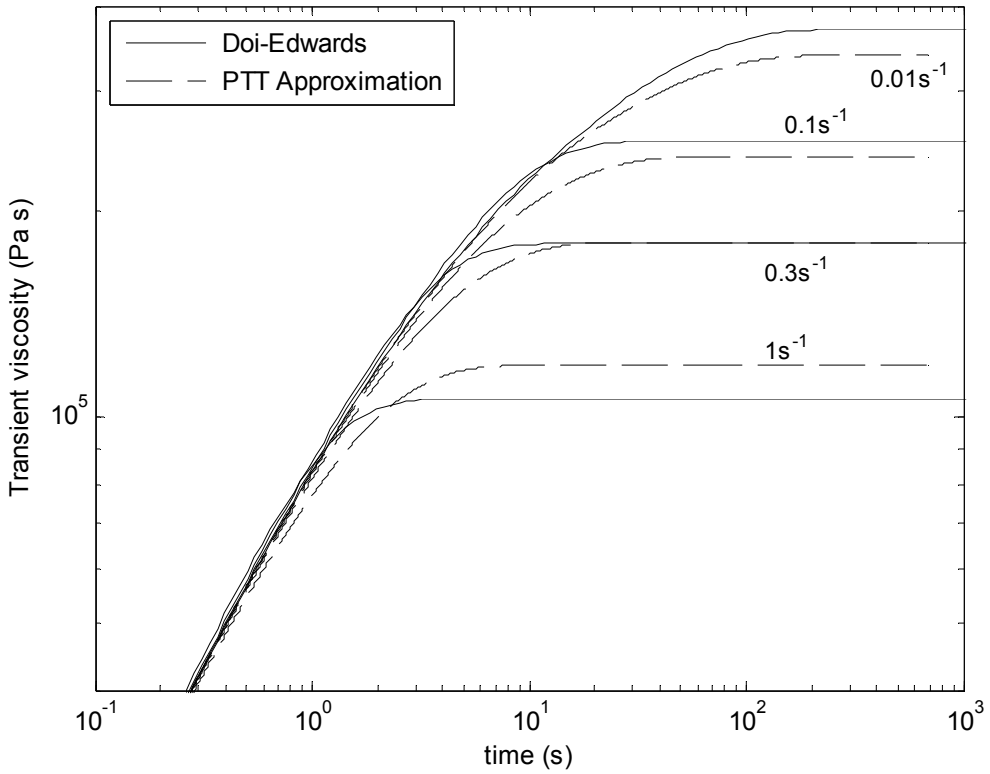

Figure 15 Comparison of the predictions in transient extension of the Doi-Edwards model and the multi-mode PTT approximation with a value of $\varepsilon = 0.33$.

A recent paper, Ref. [27], gives data for the same polymer (CAS 0993-53-6 from Aldrich) in startup flow, relaxation and in reversing flow. In the startup and relaxation experiments the polymer was stretched uniaxially until a Hencky strain of 3 was reached, and then this strain was held as the polymer relaxed. This was repeated for a range of extension rates (all at 120°C). Model predictions were shown to be close to experiment using a recent MSF model [28], and predictions from the Doi-Edwards model were also shown. Figure 16 shows the startup and relaxation data taken from Ref. [27] along with predictions from the PTT approximation, and also Doi-Edwards predictions from [27].

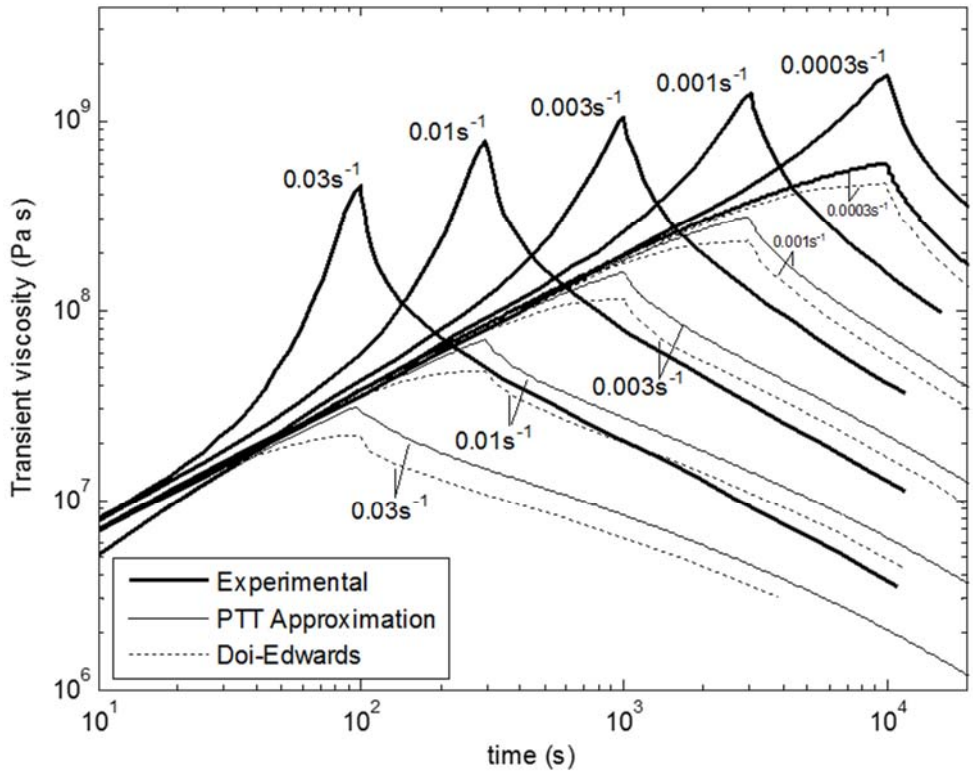

Figure 16 Experimental startup and relaxation data at 120°C from Ref.[27], compared with predictions from the PTT approximation (using an 8-mode relaxation spectrum) and Doi-Edwards predictions from Ref.[27]

At each extension rate the experimental results show considerable strain hardening, with the peaks corresponding to a Hencky strain of 3, followed by stress relaxation. Although the PTT approximation can't give this level of strain hardening (it gives a response more similar to the Doi-Edwards), the gradients of stress relaxation of the PTT approximation are seen to be realistic and comparable to experimental and Doi-Edwards results. At low values of time (around 10 seconds) three distinct curves are visible. The highest curve is from experimental data at rates of $0.03s^{-1}$ and $0.01s^{-1}$, the middle curve is from the experimental results at rates of $0.003s^{-1}$ $0.001s^{-1}$ and $0.0003s^{-1}$ (and it also contains the Doi-Edwards predictions). The lowest curve at low values of time is from the PTT approximation (using the 8 mode relaxation spectrum, as given in Table 1). The Doi-Edwards curves had been generated using a 15 mode relaxation spectrum as given in Ref. [27]; upon repeating the PTT approximation computation using this same 15 mode spectrum the PTT approximation results coincided with the Doi-Edwards curves at low times (to graphical scale); the heights of the peaks and the gradients of the relaxation slopes were only slightly changed from the 8 mode predictions.

It is worth noting that Ref. [27] also gives reversing flow data for the same polymer. However because the PTT approximation uses the magnitude of the deformation rate (Eq. 3) it loses the 'direction' of deformation and so won't respond accurately in reversing flows. This factor shouldn't be important in the current simulations as reversing flow is not a notable characteristic of the flows; this situation seems likely to be the case in many industrial GAIM flows, but needs to be considered for each process.

The multi-mode model was applied to the simulation of gas penetration in a cylinder of viscoelastic material as described in Section 4. It is to be noted that the only 'fitting' procedure (in addition to using the rheometric spectrum of the material) was finding the value of ε giving best correspondence to Doi-Edwards behaviour in transient extension. The results are shown in Fig. 17. The multi-mode simulation shows a clear drop in fractional coverage as the Deborah Number increases. The experimental data shows a significantly greater drop than the simulation but the tendency is correct, and without ambiguity in the choice of time constant. The difference between the experimental data and the multi-mode approximation data is comparable to the difference between the full Doi-Edwards simulations and the experimental data.

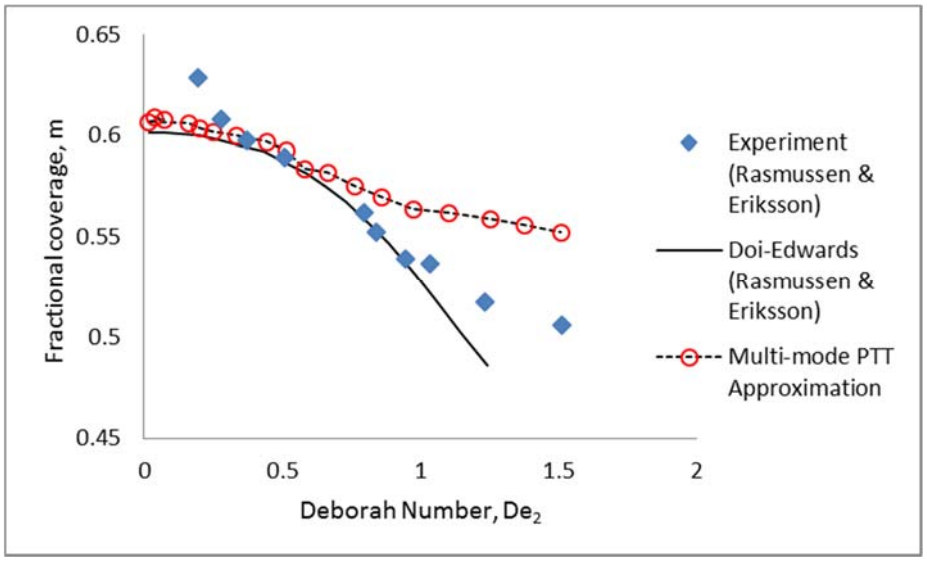

Figure 17 Comparison of Multi-mode PTT Approximation with experimental results and Doi-Edwards simulations of ref. [15].

Figure 18 shows corresponding plots of the bubble outline (c = 0.5 contour) and the scalar stress, $\overline{\tau}$ for the shear-thinning multi-mode fluid. The fractional coverage is significantly lower than for the plot shown for the Boger fluid (Fig. 7). For Fig. 18 the increment between contours of stress level is chosen to give the same number of contours in the polymer to the right of the advancing bubble as in Fig. 7, and so a contour level represents the same fraction of wall stress in both of Figs. 7 and 18. Comparing the stress patterns between Figs. 7 and 18, it is noticeable that there are a greater number of contour lines dipping in front of the bubble (ie to the right of the c = 0.5 contour) for the shear-thinning fluid (Fig.18). This shows that the stress in front of the bubble tip is a greater fraction of the wall shear stress for the shear-thinning fluid. This point is consistent with shear-thinning causing reduced resistance near the walls (where shear rate is high), which in turn is consistent with shear-thinning causing reduced fractional coverage, as it would tend to make progress near the wall easier than for a fluid without shear thinning (such as the Boger fluid of Fig. 7).

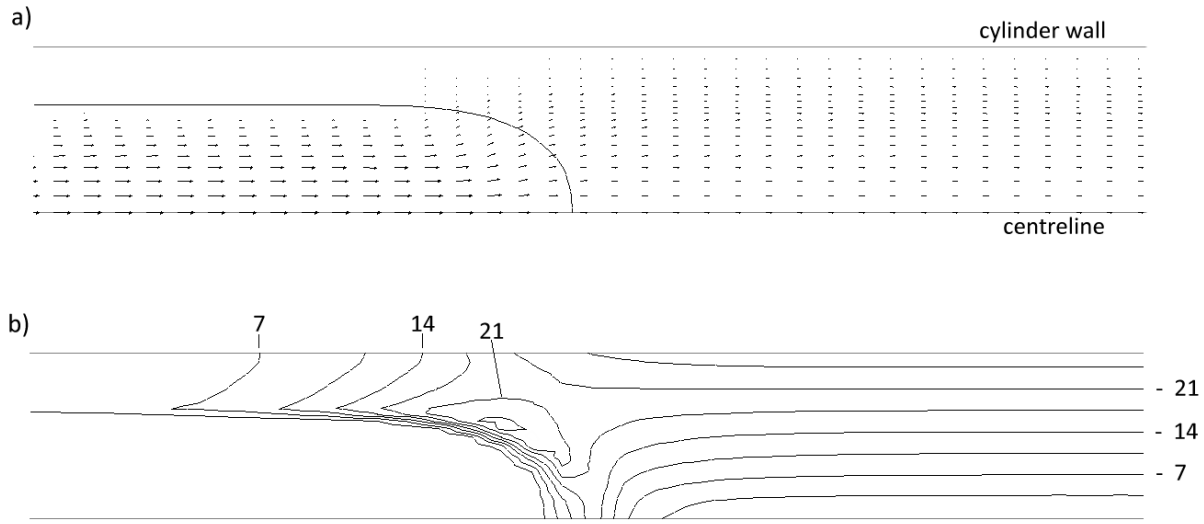

Figure 18 Concentration, c, velocity and scalar stress for multi-mode simulation at a Deborah number, De_2, of 0.762 (fractional coverage, *m*=0.575). a) Contour of c =0.5 and velocity vectors around the bubble front. b) Corresponding contours of scalar stress, numeric labels give the stress in kPa.

7. Discussion and Conclusions

An approximation to the PTT constitutive equations has been developed with the aim of giving low computational cost simulation with significant viscoelastic characteristics. The model was applied to simulations of Gas Assisted Injection Moulding, using the pseudo-concentration method, for which there are experimental results and some simulation results in the literature. The method was used to simulate the displacement of viscoelastic fluids in constant cross-section tubes, and determine the residual wall thickness and so the fractional coverage after displacement of the viscoelastic fluid by the gas.

In a simulation of a Boger fluid the simulation gave a pronounced rise in fractional coverage, beginning at a Deborah number of approximately 1, which agrees well with experimental results from Huzyak & Koelling [24]. This is significant as increased fractional coverage is associated with elasticity [18] and shows the PTT approximation is replicating this effect. The author is not aware of a comparable match to this data using simulation. Simulations with shear-thinning viscoelastic fluids have proven more variable, for example Dimakopoulos & Tsamaopoulos [18] found a slight increase in fractional coverage with increasing Deborah number, whereas Rasmussen & Eriksson found a marked decrease in fractional coverage.

The simulations of Rasmussen & Eriksson were replicated, but using the PTT approximation with a single time-constant instead of the Linear Molecular Stress Function (LMSF) models with a Baumgaertel, Schausberger and Winter (BSW) memory function; in some simulations they used the LMSF model with a maximum stretch parameter of unity which makes it identical to the Doi-Edwards (D-E) model. The PTT approximation could not replicate the strong strain hardening of the uniaxial rheological data, however the D-E model had given

the best results (in comparison to experimental results) in the simulations in ref. [15]. Hence the model was fitted to the D-E model. There is room for uncertainty when choosing a single relaxation time constant to represent viscoelastic fluid that is more convincingly represented by a spectrum of relaxation time-constants; two 'plausible' values of single time-constant were deduced and a fit to transient extensional data was used to find a value for the damping parameter, ε, in each case. In their simulations Rasmussen & Eriksson used a complex definition of Deborah number that is suitable for fluids with a spectrum of time constants; an approximate relationship was deduced to allow this complex Deborah number (denoted De_2 in this work) to be interpreted in simulations that use a single time-constant. From the current simulations it is noteworthy that the two different but 'plausible' time constants gave qualitatively different results. It was found that the shorter time constant gave a reduction in fractional coverage with Deborah number, in alignment with experimental data, whereas the longer time constant gave a rise in fractional coverage – this shows the sensitivity of single time-constant. To resolve the choice of time constant, and hence essentially resolve whether the PTT approximation gives an increase or decrease of fractional coverage, a corresponding multi-mode PTT approximation was developed.

The multi-mode PTT approximation used the full relaxation spectrum (derived from the G' and G'' data of Rasmussen & Eriksson [15]), and was fitted to the parameter-free D-E model by choosing the value of the single damping parameter, ε, that gave the best overall fit. The multi-mode PTT approximation gave reducing fractional coverage with increasing Deborah number, thus resolving the difficulty inherent in choosing which single time-constant to use (of several plausible candidates). It is perhaps significant that the single-mode simulation that used the relaxation time that gave the best direct fit to G' and G'' data matched the multi-mode results most closely.

The simulations were run de-coupling the viscoelastic stress and the pseudo-concentration equations from the main Stokes type solution of *u-v-w-p*. In this way the computational cost was little higher than the cost of a time-stepping power-law type computation (approximately 10% higher). The model succeeded in predicting quite accurately the fractional coverage behaviour of a Boger fluid, and in multi-mode form the qualitative behaviour of a shear thinning polymer. The model is an approximation that captures some aspects of viscoelastic flow but not all, for example there is no prediction of Normal Stress Difference in shear flow, and reversing flows won't be accurately captured as the approximation implements the time-integrated stress as a scalar viscosity. The model successfully captures stress build-up and associated elasticity effects (as well as shear-thinning) and has applications where these are dominant effects. Additionally it should be practicable to implement the PTT approximation in a commercial CFD package, provided the package permits a 'user defined' transport equation (for the scalar stress) and a user-defined viscosity input.

A particular aspect of the pseudo-concentration method is of interest here. The simulation implementations of Dimakopoulos & Tsamaopoulos [18] and Rasmussen & Eriksson [15] were both Lagrangian (moving mesh) based methods and agree on a low Deborah number (Newtonian) fractional coverage value of 0.60, whereas the current pseudo-concentration simulations give 0.61 for the same value. In the Lagrangian methods the polymer-gas interface is aligned with element edges and the different material properties are applied either side of the element edges. In the pseudo- concentration method the interface is (normally) defined as the contour of concentration = 0.5, and the different properties of the

materials are applied gradually by a linear interpolation across the boundary from pure polymer (concentration = 1) to gas (concentration = 0); this boundary is normally 3 or 4 elements across. It is reasonable to deduce that the material properties are applied less exactly (in a positional sense) than in the Lagrangian methods, and so some loss of precision can be expected from Eulerian pseudo-concentration implementations. However the pseudo-concentration method has the significant strength that it extends to complex 3D geometries without the re-meshing difficulties associated with most Lagrangian methods.

Taking all into account the PTT Approximation model has shown itself to be effective as a predictive tool in GAIM with the ability to provide transient viscosity and elasticity at low computational cost, and it has the potential to be used in other applications where such memory effects are important.

Appendix A. Convergence with mesh and time-step

Convergence was investigated using three meshes. Mesh 1 (as used for the main simulations in this work) had 18000 elements and 20412 nodes, and two meshes with fewer elements were produced from this using the method of Ref.[29]. Mesh 2 was created by halving (to nearest integer) the number of elements along each dimension of Mesh 1, and had 1920 elements and 2501 nodes. Mesh 3 with 729 elements and 1036 nodes was created by using 1/3rd of the number of elements along each dimension of Mesh 1 (a coarser mesh had been attempted by halving the number of elements along each dimension of Mesh 2, but this didn't give satisfactory results in simulations).

The three meshes were used for the Boger fluid problem at a Deborah number (De_1) of 2.09, and for the shear-thinning fluid using a single time constant of 2.2 sec at a Deborah number $\left(De_1\right)$ of 16.74, and also for the multimode approach at a Deborah number $\left(De_2\right)$ of 0.762 . These points were chosen as they are representative points around the centre of the rising and falling parts of the curves in Figures 6, 14 and 17, respectively. The time step, Δt for each was kept such that $U\,\Delta t = \Delta X\,/10$, where U was the peak speed along the centreline and X was the length of elements along the centreline. The results are in Table A.1.

	Elements, N	Boger fluid $\begin{pmatrix}\lambda = 0.37s, \varepsilon = 0 \\ De_1 = 2.09\end{pmatrix}$ Fractional coverage, m	Shear-thinning fluid, single mode $\begin{pmatrix}\lambda = 2.2s, \varepsilon = 1.3, \\ De_1 = 16.74\end{pmatrix}$ Fractional coverage, m	Shear-thinning fluid, multi-mode $\begin{pmatrix}\varepsilon = 0.33, \\ De_2 = 0.762\end{pmatrix}$ Fractional coverage, m
Mesh 1	18000	0.6908	0.5882	0.5751
Mesh 2	1920	0.7112	0.5644	0.5610
Mesh 3	729	0.7288	0.5731	0.5537

Table A.1 Values of fractional coverage, m ,for three meshes of different element density for a Boger fluid and a shear-thinning fluid.

Ref. [29] gives a method for deducing convergence order by fitting to an equation of the form

$$m = m_0 + \upsilon\left(N^{-\frac{1}{3}}\right)^{\alpha}, \qquad \text{Eq (A.1)}$$

where m_0, υ and α are unknowns; N is the number of elements in a mesh and m is the fractional coverage. The term $N^{-\frac{1}{3}}$ is a gauge of element dimension (for a 3D mesh). Substituting values of m from three columns of Table A.1 with their corresponding N values into Eq. (A.1) gives three equations which can be solved for the unknown values for that column. The values of α were found to be approximately 1.4 and 0.3 for the first and third columns of fractional coverage values, though no solution could be found for the second column, indicating that the values don't fit the form of Eq. (A.1). The average for the two values is 0.85 which suggests the method converges approximately linearly with element size; this seems reasonable as linear elements were used in the simulations.

Comparing differences between the two finest meshes (Mesh1 and Mesh 2) gives an average difference in *m* of 0.017; this suggests 1.7% as indicative of the likely worst error for the finer mesh (as used in the main simulations).

Time-step convergence was checked using the finest mesh, Mesh 1, with time steps expressed as a fraction of the limit from the Courant criterion

$$\Gamma = \frac{\Delta X}{U} \qquad \text{Eq (A.2)}$$

where U is the peak speed along the centreline and X is the length of elements along the centreline. Simulations were conducted with $\Delta t = \Gamma/10$, $\Delta t = \Gamma/7$ and $\Delta t = \Gamma/5$. The results are given in Table A.2.

$\frac{\Delta t}{\Gamma}$	Boger fluid $\left(\begin{matrix}\lambda = 0.37s, \varepsilon = 0, \\ De_1 = 2.09, \Gamma = 0.017s\end{matrix}\right)$ Fractional coverage, *m*	Shear-thinning fluid, single mode $\left(\begin{matrix}\lambda = 2.2s, \varepsilon = 1.3, \\ De_1 = 16.74, \Gamma = 0.013s\end{matrix}\right)$ Fractional coverage, *m*	Shear-thinning fluid, multi-mode $\left(\begin{matrix}\varepsilon = 0.33, \\ De_2 = 0.762, \Gamma = 0.26s\end{matrix}\right)$ Fractional coverage, *m*
1/10	0.6908	0.5882	0.5751
1/7	0.6926	0.5895	0.5765
1/5	0.6941	0.5910	0.5773

Table A.2 Values of fractional coverage, *m*, for three different time steps expressed as a fraction of the Courant criterion

Ref. [29] gives a similar method for deducing convergence order for time-step by fitting to an equation which can be written

$$m = m_0 + \upsilon\left(\frac{\Delta t}{\Gamma}\right)^{\alpha}, \qquad \text{Eq (A.3)}$$

where m_0, ν and α are unknowns. Substituting the three corresponding pairs of values for $\Delta t/\Gamma$ and m from Table A.2 into Eq. (A.3) yielded values of α of approximately 0.7 and 1.3 for the first and second columns of fractional coverage, though no value could be found for the third column. The average is 1.0 which suggests the method converges approximately linearly with time-step size. This seems reasonable as the backwards-differencing time-stepping that was used in the simulations has first-order accuracy [22]. The differences between by the two shortest time-steps are small compared to the differences between the two finest meshes.

Haagh et al. [1] reported the need to keep time steps much smaller than the Courant limit for the pseudo concentration method. For illustration the Boger fluid simulations were continued for $\Delta t/\Gamma =$ 0.3, 0.5 and 1.0, giving values for fractional coverage of 0.6924, 0.6776 and 0.6410 respectively. These show the results change very rapidly after a $\Delta t/\Gamma$ value of approximately 0.3, and illustrate the point made by Haagh et al. A likely explanation is that large values of $\Delta t/\Gamma$ allow the bubble front to advance without due regard for the stress gradients in front of it.

References

[1] Haagh, G.A.A.V., Zuidema, H., Van De Vosse, F.N., Peters, G.W.M., and Meijer, H.E.H. Towards a 3-D Finite Element Model for the Gas-Assisted Injection Moulding Process. Int. Polym. Proc., 1997, 12 /3, 207-215

[2] Haagh, G.A.A.V., Peters, G.W.M., Van De Vosse, F.N., and Meijer, H.E.H. A 3-D finite element model for gas-assisted injection Molding: Simulations and Experiments. Polym. Eng. Sci., 2001, 41, 449-465.

[3] Yang, B., Fu, X.-R., Yang, W., Liang, S.-P., Hu, S., and Yang, M.-B. Simulation of phase-change heat transfer during cooling stage of Gas-Assisted Injection Molding of High-Density Polyethylene via enthalpy transformation approach. Polym. Eng. Sci., 2009, 49, 1234-1242

[4] Zheng, G.-Q., Li, Q., Chen, J.-B., Shen, C.-Y., Yang, W., and Yang, M.-B. Gas-assisted injection molded polypropylene/glass fiber composite: foaming structure and tensile strength. Polym.-Plast. Tech. Engn., 2009, 48 (2), 170-177.

[5] T. Pudpong, P. Buahom, S. Areerat, W. Rungseesantivanon, I. Satoh, and T. Saito, “The effects of processing parameters on the residual wall thickness distribution at the sharp angle corner of water assisted injection molded parts,” Int. Polym. Process., vol. 28, no. 5, pp. 528–540, 2013.

[6] H. Park and B. Rhee, “Effects of the viscosity and thermal property of fluids on the residual wall thickness and concentricity of the hollow products in fluid-assisted injection molding,” Int. J. Adv. Manuf. Technol., vol. 86, no. 9–12, pp. 3255–3265, 2016.

[7] K. Alba and I.A. Frigaard, Dynamics of the removal of viscoplastic fluids from inclined pipes, J. non-Newt. Fluid Mech. 229 (2016) 43-58

[8] A. Eslami, I.A. Frigaard, S.M. Taghavi, Viscoplastic fluid displacement flows in horizontal channels: Numerical simulations, J. non-Newt. Fluid Mech. 249 (2017) 79-96

[9] M. Zare, A. Roustaei and I.A. Frigaard, Buoyancy effects on micro-annulus formation: Density stable displacement of Newtonian-Bingham fluids, J. non-Newt. Fluid Mech. 247 (2017) 22-40

[10] S.M. Mazahir, G.M. Velez-Garcia, P. Wapperom, D. Baird, Fiber orientation in the frontal region of a center-gated disk: Experiments and Simulation, J. non-Newt. Fluid Mech. 216 (2015) 31-44

[11] M. J. Divvela, A-C. Ruo, Y. Zhmayev, Y. L. Joo, Discretized modeling for centrifugal spinning of viscoelastic liquids, J. non-Newt. Fluid Mech. 247 (2017) 62-77

[12] A. Polynkin, J.F.T. Pittman, J. Sienz, Gas assisted injection moulding of a handle: three dimensional simulation and experimental verification. Polym. Eng. Sci., 45 (2005) 1049-1058

[13] A. Polynkin, J.F.T. Pittman, J. Sienz, Industrial application of gas assisted injection moulding: numerical predictions and experimental trials. Plastics, Rubbers and composites, 25 (2005) 236-246

[14] P. Olley, L. Mulvaney-Johnson, P.D. Coates, Simulation of the gas-assisted injection moulding process using a viscoelastic extension to the Cross-WLF viscosity model. Proc IMechE, Part E: J. Process Mechanical Engineering 225 (2011) 239–254.

[15] H.K. Rasmussen, T. Eriksson, Gas displacement of polymer melts in a cylinder: Experiments and viscoelastic simulations. J. non-Newt. Fluid Mech., 143 (2007) 1-9

[16] J.M. Roman Marin, H.K. Rasmussen, Lagrangian finite-element method for the simulation of K-BKZ fluids with third order accuracy, J. non-Newt. Fluid Mech. 156 (2009) 177-188

[17] A. Bach, H.K. Rasmussen, P.Y. Longin, O. Hassager, Growth of non-axisymmetric disturbances of the free surface in the filament stretching rheometer: Experiments and simulation, J, non-Newt. Fluid Mech. 108 (2002) 163-186

[18] Y. Dimakopoulos, J. Tsamopoulos, On the gas-penetration in straight tubes completely filled with a viscoelastic fluid, J. non-Newt. Fluid Mech. 117 (2004) 117-139.

[19] Y. Dimakopoulos, An efficient parallel and fully implicit algorithm for the simulation of transient free-surface flows of multimode viscoelastic liquids, J. non-Newt. Fluid Mech. 165 (2010) 409-424

[20] H.K. Rasmussen, Lagrangian viscoelastic flow computations using a generalised molecular stress function model. J. Non-Newt. Fluid Mech. 106 (2002) 107-120

[21] R.A. Figueiredo, C.M. Oishi, J.A. Cuminato, M.A. Alves, Three-dimensional transient complex free surface flows: Numerical simulation of XPP fluid, J. Non-Newt. Fluid Mech. 195 (2013) 88-98

[22] J.N. Reddy, An introduction to the finite element method, 2nd Edn. McGraw-Hill, New York (1993)

[23] P.M. Gresho, S.T. Chan, R.L. Lee, C.D. Upson, A modified finite element method for solving the time-dependent incompressible Navier-Stokes equations, Int. J. Num. Meth. Fluids, 4 (1984) 557-598

[24] P.C. Huzyak, K.W. Koelling, The penetration of a long bubble through a viscoelastic fluid in a tube, J. Non-Newt. Fluid Mech. 71 (1997) 73-88

[25] A. Haghtalab, G. Sodeifian, Determination of the discrete relaxation spectrum for polybutadiene and polystyrene by a non-linear regression method, Iran. Polym. J. 11/2 (2002) 107-113

[26] M.H. Wagner, H. Bastian, P. Hachmann, L. Meissner, S. Kurzbeck, H. Munstedt, F. Langouche, The strain-hardening behaviour of linear and long-chain-branched polyolefin melts in extensional flows, Rheol. Acta 39 (2000) 97-109

[27] Q. Huang, H.K. Rasmussen, Extensional flow dynamics of polystyrene melt, J. Rheol. 63 (2019) 829-835

[28] E. Narimissa, M.H. Wagner, A hierarchical multimode molecular stress function model for linear polymer melts in extensional flows, J. Rheol. 60 (2016) 625-636

[29] H.K. Rasmussen, Lagrangian viscoelastic flow computations using the Rivlin-Sawyers constitutive model. J.Non-Newt. Fluid Mech. 92 (2000) 227-243